THESIS FOR THE DEGREE OF DOCTOR OF PHILOSOPHY

Nanoscale technologies for plasmon-assisted solar light harvesting and lipid membrane composites

GUSTAV EDMAN JÖNSSON

Department of Physics
Chalmers University of Technology
Gothenburg, Sweden 2016

Nanoscale technologies for plasmon-assisted solar light harvesting and lipid membrane composites
GUSTAV EDMAN JÖNSSON

Department of Physics
Chalmers University of Technology
SE-412 96 Gothenburg
Sweden
Telephone + 46 (0)31-772 1000

Chalmers Reproservice
Gothenburg, Sweden 2016

Nanoscale technologies for plasmon-assisted solar light harvesting and lipid membrane composites

Gustav Edman Jönsson
Department of Physics
Chalmers University of Technology

Abstract

Techniques for design, manipulation and characterization of nanoscale structures provide the basis for technological advances in areas like optics, electronics and biotechnology. The aim of this thesis is to develop new nanoscale methods and design schemes that extend the applicability of nanoscale devices. In particular the design of plasmonic antennas and formation of composite structures of lipid membranes and graphene oxide (GO) are in the focus of this work.

Lipid membranes and lipid vesicles are relevant in the field of biotechnology where they are used to model cell-membranes and as carriers of various functional biological units. The ability to isolate neighboring membranes or to connect them to electrical conductors could prove valuable for future applications. With this in mind the interaction between GO and lipid membranes is studied. Results from quartz crystal microbalance with dissipation monitoring and dual polarization interferometry indicate that flakes of GO, which have negative ζ-potential, bind to lipid membranes with positive ζ-potential. Furthermore, GO induces rupture of immobilized lipid vesicles and together form composite structures in a layer-by-layer fashion. Atomic force microscopy shows that these structures are stable in air.

Metal nanoparticles host localized surface plasmon resonances (LSPR) at optical frequencies. These resonances couple to freely propagating light and greatly enhance the optical cross sections of the metal particles. Modifications of particle morphology and materials composition as well as interactions between near-by particles influence the characteristics of the LSPR. Here supported arrays of plasmonic optical antennas are designed with the purpose of light induced heating of the transparent surfaces. The optical properties of these surfaces are studied with optical spectroscopy and a method based on thermal imaging is developed to evaluate the light-to-thermal energy conversion efficiency.

Keywords: thermo-optical materials, metamaterials, thermal imaging, plasmonics, lipid membranes, graphene oxide

List of publications

Papers 1, 2, 3 and 4 are central to this thesis work and are appended.

Paper 1

Graphene oxide and lipid membranes:
interactions and nanocomposite structures
Rickard Frost, Gustav Edman Jönsson, Dinko Chakarov, Sofia Svedhem
and Bengt Kasemo,
Nano Letters, 12 (7), 3356, 2012

My contribution: I took part in planning the experimental work. I participated in doing main parts of the experiments. I prepared parts of the manuscript.

Paper 2

Nanoplasmon-enabled macroscopic thermal management
Gustav Edman Jönsson, Vladimir Miljkovic and Alexandre Dmitriev
Scientific Reports, 5, 5111, 2014

My contribution: I planned the experiments together with AD, I developed experimental methods, I did all the experiments, I developed a numerical model together with VM and I wrote the manuscript together with AD

Paper 3

Solar transparent radiator using optical antennas
Gustav Edman Jönsson, Tavakol Pakizeh, Manoj Jaysankar, Lianming Tong,
Vladimir Miljkovic and Alexandre Dmitriev
Submitted

My contribution: I planned the experiments together with AD. All experiments were done by me directly or under my supervision. I wrote the manuscript together with AD

Paper 4

Absorbing nanoplasmonics with naturally abundant materials for solar energy harvesting
Gustav Edman Jönsson, Tavakol Pakizeh and Alexandre Dmitriev
In manuscript

My contribution: I planned and performed all the experiments. I conceived the numerical simulations. I wrote the manuscript together with AD.

Other papers not included in this thesis.

Nanostructures for Enhanced Light Absorption in Solar Energy Devices
Gustav Edman Jonsson, Hans Fredriksson, Raja Sellappan
and Dinko Chakarov
International Journal of Photoenergy, 2011 , art. no. 939807

Contents

List of acronyms and symbols

Below is a compilation of symbols and acronyms occurring in this work.

AFM	Atomic Force Microscope
c	Speed of light
∅	Diameter
E	Electric field strength
EELS	Electron Energy Loss Spectroscopy
$\varepsilon = \varepsilon' + i\varepsilon''$	Complex permittivity
ESEM	Environmental Scanning Electron Microscope
FDTD	Finite Difference Time Domain
FEM	Finite Element Method
HCL	Hole-Mask Colloidal Lithography
h	Planck's constant
I	Irradiance
J	Current density
k	Wave number
λ	Wavelength
LSPR	Localized Surface Plasmon Resonance
ω	Angular frequency
PDDA	Polydiallyldimethylammonium
PMMA	Polymethylmethacrylate
PVD	Physical Vapor Depositon
QCM-D	Dissipation Monitored Quartz Crystal Microbalance
SEM	Scanning Electron Microscope
σ	Electric conductivity OR optical cross-section

1 Introduction

Nanotechnology regards the ability to process and analyze objects having at least one dimension on the nanometer length scale.[1] The benefits of working on the nanoscale include one obvious: Miniaturization that makes it possible to fit more objects in the same area. This is especially evident in data storage where the storage capacity increases with the ability to miniaturize the storage devices. A second, perhaps less obvious, benefit with working on the nanoscale is the possibility to fine-tune the physical properties of a material. This can often be done just by changing its size or shape on the nanoscale. Such changes in physical properties are quite common, and the resulting materials are called nanomaterials.

One illustrative example is what happens to carbon in the form of graphite. Ultimately thin graphite, i.e. when only one layer of carbon atoms remains, goes under the name graphene.[2] Graphene has widely separate physical properties from graphite and currently provides the basis for a teeming field of research.[3]

Metals provide a second example. Pieces of metal on the human scale are opaque and reflective but metal particles with dimensions on par with the wavelength of light have highly wavelength selective optical properties; they are transparent to some colors (wavelengths) but reflect and absorb others.[4]

In order to produce nanometer sized structures in a reproducible way one relies on precise experimental methods and protocols. Over the years the number of these methods have grown and found wider applicability so that a great range of structures are possible to make and utilize. Still the number of available methods poses a restriction on what types of structures and functionalities can be realized. Therefore finding ways to fabricate new types of structures with new types of functionalities is always one of the focuses of nanoscience research.

The rest of this chapter introduces the nanomaterials lipid bilayers, graphene oxide and plasmonic metal nanoparticles. Also the contribution of this thesis to these fields is introduced.

1.1 Lipid bilayers and graphene oxide.

The human body is a complex machinery consisting of many organs that are strongly interdependent. Each organ is again a complex machinery consisting of different cell types. Every cell type has a specific functionality but all share similarities. All human cells are enclosed by a protective shell called the cell membrane. This membrane consists of a double layer of amphiphilic molecules. An amphiphilic molecule has one part that is attracted to water and another that is rejected by water. In the cell membrane the amphiphilic molecules arrange themselves with their hydrophobic (water-rejected) parts facing each other in the middle of the membrane and their hydrophilic (water-attracted) parts pointing out of the membrane.[5] Figure 1.1 illustrates this type of arrangement.

Human cell membranes consist mostly of a type of amphiphilic molecules called phospholipids. Phospholipids have a hydrophilic head consisting of glycerol phosphate with polar groups and a hydrophobic double tail consisting of fatty acids. The double tail makes it energetically favorable for this type of lipids to arrange themselves in the form of a membrane. Other types of lipids may arrange themselves in other ways. As it is energetically unfavorable to expose the hydrophilic membrane edges the membranes tend to close themselves in water and form spherical liposomes,[5] c.f. Figure 1.1.

Interactions between a cell and a foreign entity, for example, a nanoparticle, can affect the functionality of the cell and thus have great consequences to both the cell and the organism. As cell-particle interactions initiate at the cell membrane a natural interest is focused on studying interactions between lipid bilayers and various biological and non-biological (nanoscopic) entities.

Supported lipid bilayers (SLBs) are the practical models to use when making controlled experiments related to the cell membranes. SLBs are membranes with controlled lipid composition that form on a flat surface, commonly SiO_2.[6] In this arrangement they can easily be characterized by surface probing techniques like AFM or QCM-D. [7, 8]

Part 1 of this thesis (Paper 1) investigates the interaction between SLBs having various lipid compositions and graphene oxide (GO). GO is a form of single-sheet carbon (graphene) having OH (hydroxide) and COOH (carboxyl) side groups. Because the functional groups disrupt the π-bonds of graphene, GO is not electrically conducting like pristine graphene but is instead polar and soluble in water. GO can be reduced to obtain graphene.[9]

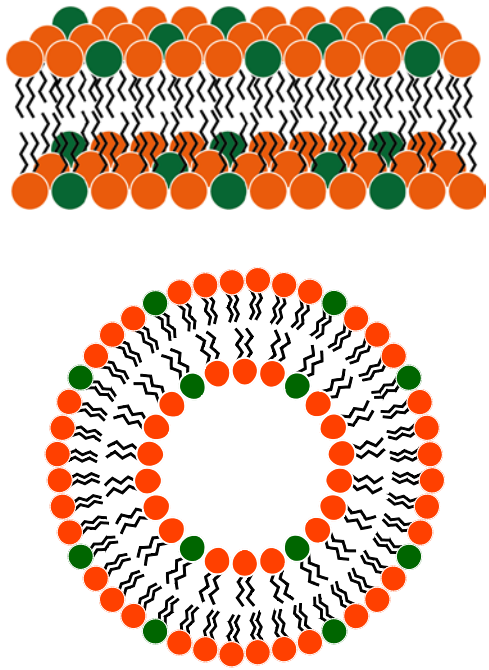

Figure 1.1 Schematic view of amphiphilic molecules arranged in bilayers. The solid balls and zig-zag double lines correspond to the hydrophilic and hydrophobic parts respectively. Different colors represent different chemical compositions of the hydrophilic ends. The upper part of the figure illustrates a section of a membrane. The bottom part illustrates a cross-section of a liposome.

Interactions between lipid bilayers and GO are of interest to study for several reasons. As GO is water-soluble it can easily enter the body. Any health issues or potential usage as drug carrier relies on the interaction with the cell membrane. There has also been activity in combining lipid membranes with graphene and carbon nanotubes (CNTs) to form functional bio-devices[10, 11] which makes the interaction interesting also from a technological point of view. This work aims to elucidate the fundamental characteristics of such interactions and to characterize physical properties of resulting structures with the purpose to build a foundation for future research.

1.2 Plasmonic metal nanoparticles and nanoantennas

Light, ranging in energy from infrared (IR) through the visible (VIS) to ultraviolet (UV), is a ubiquitous electromagnetic wave. It is an indispensable carrier of energy and information. Simply put: Without light we would freeze to death, blind.

In order to make technological use of light it must be captured. Plasmonic metal nanoparticles, that host the collective electron oscillations called plasmons, are highly interesting for this purpose as they have large optical cross-sections that can be tuned with respect to light energy, spectral line-width and angle of light incidence.[12-17] As a consequence plasmonic materials help realize compact light-harvesting devices with rich design possibilities.[18] Furthermore, new methods of nanofabrication pave the way for cheap production of large area plasmonic surfaces[19] bringing this concept closer to commercial realization.

Suggested applications of this type of surfaces span, to name a few, spectral and polarization sensitive bolometers,[19, 20] Förster resonant energy transfer,[13] sensing,[16, 17] surface enhanced Raman scattering,[16] controlled thermal emission for thermo-photovoltaics[12, 14, 21, 22] and conversion of light into heat[15].

Plasmonic optically driven heat sources, apart from being highly tunable also offer new functionality. Examples of where heat generated via light absorption in plasmonic metal nanoparticles offers new or improved functionality include increased chemical reactivity,[23] enhanced vapor formation offering a route to efficient light-driven distillation,[24, 25] assisted CVD for fabrication of nanostructures,[26, 27] focused magnetic recording (HAMR),[28] assisted nano-fluidics,[29] 'nano-blade' for cutting cell membranes,[30] control of cell migration [31] and medical treatments[32-37]. Papers 2, 3 and 4 of this thesis deal with plasmonic materials that transform light into heat

The papers concern the ability to tune the optical properties of plasmonic absorbers. Focus lies on the absorption of sunlight. In technical terms that is broadband absorption of light with energies predominantly in the visible and infrared regimes and with relatively low intensities so that no temperature gradients between particles and their surrounding are expected.

Paper 2 presents a passive method to measure the temperature increase of a transparent substrate due to plasmon assisted light to heat conversion in metasurfaces consisting of discrete plasmonic nanoparticles. Absorbed power is quantified from the dynamics of the temperature increase. Using this method the heat transformation efficiency is evaluated for surfaces comprising particles with different shapes and material composition.

Paper 3 builds on the conclusions from paper 2 and extends the particle geometries to stacked architectures – plasmonic nanoantennas. Individual geometries of the respective antenna elements induce the directionality along the light propagation. Hereby directionality in light to heat conversion efficiency can be obtained. The paper also explores the possibility to apply the plasmonic particles to window coatings.

Finally, paper 4 capitalizes on the functional roles of the respective nanoantenna elements to further boost the solar absorption in these radiator surfaces and

explores the possibility to build plasmonic antennas from naturally abundant materials.

These papers have the common aim to explore the possibility of producing absorbing, transparent, surfaces built from discrete functional entities - nanoantennas. The purpose of such surfaces is first-hand to improve the thermal economy of buildings with large glass facades.

2 Background check

2.1 Optical response of nanoscopic metal particles

Light is an electromagnetic wave that is, to great accuracy, described by Maxwell's equations that connect the electric and magnetic fields and currents.[38] The optical response of a metal nanoparticle in an environment can thus be determined by solving Maxwell's equation for the specific geometry and material constants. Analytical solutions for spherical particles in a homogeneous environment were provided by Gustav Mie in 1908.[39] For other geometries either approximations or numerical methods are used. The material constants put into the equations comprise the respective dielectric functions of the involved materials. Dielectric materials are sometimes defined by using the alternative, but equivalent, refractive index.

Choosing the appropriate dielectric function for a metal is not always a straightforward task. If it is calculated, the Drude model[40] is commonly used although it suffers from drawbacks. One major drawback is that the model does not account for the interband transitions of electrons. As several metals have interband transitions in the regions where plasmonic resonances occur, any solution to Maxwell's equations based on Drude dielectric functions will not be entirely correct. Another common approach is to use tabulated experimentally obtained values for the dielectric function. Common values are those obtained by Johnson & Christiy[41, 42] or Palik[43] .

Maxwell's equations

Maxwell's equations bundle together the fundamental physical laws of electromagnetism in a coherent form.[38, 44] Without discussions of their physical meanings the four central equations are given below.

Coulomb's law

$$\overline{\nabla} \cdot \overline{\mathrm{E}} = -4\pi e n \tag{2.1}$$

Faraday's law of induction

$$\overline{\nabla} \times \overline{\mathrm{E}} = -\frac{1}{c}\frac{\partial \overline{B}}{\partial t} \tag{2.2}$$

Gauss' law of magnetism

$$\overline{\nabla} \cdot \overline{\mathrm{B}} = 0 \tag{2.3}$$

Maxwell's adjusted Ampère's law

$$\overline{\nabla} \times \overline{\mathrm{B}} = \frac{4\pi \overline{J}}{c} + \frac{1}{c}\frac{\partial \overline{E}}{\partial t} \tag{2.4}$$

Here e is the elementary charge, n is the number concentration of charge, c is the speed of light and J is current density.

It is possible to separate n into n_{ext} and n_{int} for external and internal charges, where external charges drive the system and the internal charges are responding. A polarization field can now be defined as follows.

$$\overline{P}(t) = \int^{t} dt' \overline{J}_{int}(t') \tag{2.5}$$

Here J_{int} represents the current density from internal charges contribution. The continuation equation states that the following holds: (applying the divergence operator on both sides of (2.4))

$$-e\frac{\partial n_{int}}{\partial t} = -\overline{\nabla} \cdot \overline{J}_{int} \tag{2.6}$$

Consequently, the divergence of the polarization field becomes

$$e n_{int} = \overline{\nabla} \cdot \overline{P} \tag{2.7}$$

A displacement field can be defined as follows

$$\overline{D} = \overline{E} + 4\pi \overline{P} \tag{2.8}$$

Inserting this displacement field in the original Maxwell's equation gives

$$\overline{\nabla} \cdot \overline{D} = -4\pi e n_{ext} \tag{2.9}$$

$$\overline{\nabla} \times \overline{B} = \frac{4\pi \bar{J}_{ext}}{c} + \frac{1}{c}\frac{\partial \overline{D}}{\partial t} \tag{2.10}$$

Linear relationships between the electric field and current density and displacement field are given by the conductivity σ and the dielectric function/constant ε according to:

$$\bar{J}(\bar{r}, t) = \sigma * \overline{E}(\bar{r}, t) \tag{2.11}$$

$$\overline{D}(\bar{r}, t) = \varepsilon * \overline{E}(\bar{r}, t) \tag{2.12}$$

The Fourier transforms of which are:

$$\bar{\mathrm{J}}(\bar{\mathrm{k}}, \omega) = \sigma(\bar{\mathrm{k}}, \omega)\overline{\mathrm{E}}(\bar{\mathrm{k}}, \omega) \tag{2.13}$$

$$\overline{\mathrm{D}}(\bar{\mathrm{k}}, \omega) = \varepsilon(\bar{\mathrm{k}}, \omega)\overline{\mathrm{E}}(\bar{\mathrm{k}}, \omega) \tag{2.14}$$

Finally, the following relationship can be deduced by combining equations from above:

$$\varepsilon(\bar{\mathrm{k}}, \omega) = 1 + \frac{4\pi \mathrm{i}}{\omega}\sigma(\bar{\mathrm{k}}, \omega) \tag{2.15}$$

Equations (2.13) and (2.14) are central for solving Maxwell's equations. Equation (2.15) is a powerful relationship when calculating the dielectric function.

Solutions and approximations for metal nanoparticles

Solving Maxwell's equations for small particles, with diameters considerably smaller than the wavelength of light, it is practical to assume that the exciting electric field is constant in space but varying in time. This assumption is known as the quasi-static approximation.

Solutions in the quasi static approximation can be found by using the electric potential Φ. The relation between the electric potential and the electric field is given by:

$$\nabla\Phi = -\overline{E} \tag{2.16}$$

For a metal particle in a static electric field Laplace's equation is valid, stating that:

$$\nabla^2\Phi = 0 \tag{2.17}$$

Linear combinations of spherical harmonics give the general solution for this equation with spherical symmetry.[45] For simplicity only the lowest order term ($\ell = 1$) of the harmonics is used here. Higher order terms will include higher order oscillatory modes in the solution. The quadrupolar mode is an example that is prominent in larger spherical particles. However, for non-spherical particles it is effectively quenched.[45] It is not relevant in this thersis.

Assigning different dielectric functions to sphere and environment and paying heed to the boundary conditions at the interface between sphere and environment as well as at infinite distance from the sphere one arrives at specific solutions.

$$\Phi_{r\leq a} = -\frac{3\varepsilon_e}{\varepsilon_p + 2\varepsilon_e} E_0 r\ cos\,\theta \tag{2.18}$$

$$\Phi_{r>a} = -E_0 r\cos\theta + \frac{\varepsilon_p - \varepsilon_e}{\varepsilon_p + 2\varepsilon_e} E_0 a^3 \frac{\cos\theta}{r^2} \tag{2.19}$$

Here, a is the radius of the sphere, E_0 is the amplitude of the driving electric field and θ is the angle between the position vector r and the electric field vector. ε_e and ε_p are the dielectric constants of the environment and particle respectively.

Equation (2.19) describes the total electric potential outside the metal sphere. This potential can be regarded as a superposition of the driving electrical potential and potential arising from a dipole. The dipole being the polarized metal sphere. It is possible to rewrite the contribution from the dipole in the following form.

$$\Phi_{r>a} = -E_0 r\cos\theta + \frac{\overline{p}\cdot\overline{r}}{4\pi\varepsilon_p r^3} \tag{2.20}$$

$$\overline{p} = \varepsilon_p \alpha \overline{E_0} \tag{2.21}$$

$$\alpha = 4\pi a^3 \frac{\varepsilon_p - \varepsilon_e}{\varepsilon_p + 2\varepsilon_e} \qquad (2.22)$$

The vector $\overline{p}$ corresponds to the dipole moment induced by the electric filed. Its magnitude is proportional to the polarizability, α, of the metal nanoparticle. As the dielectric functions are complex-valued information about both amplitude and phase is contained in the expression. Figure 2.1 shows amplitude and phase for the polarizability of a small gold nanosphere. A central property of the polarizability of small metal spheres is that it becomes singular when the following condition is fulfilled.

$$\varepsilon_p = -2\varepsilon_e \qquad (2.23)$$

This polarization enhancement of the particle is commonly referred to as a localized plasmon resonance or LSPR for short. As ε_p varies as a function of wavelength the condition (*2.23*) can be fulfilled for various values of ε_e, i.e. the dielectric function of the environment, albeit at different wavelengths. This property makes plasmonic nanoparticles potent sensors for detecting changes in the dielectric function of the environment, as mentioned in the introduction.

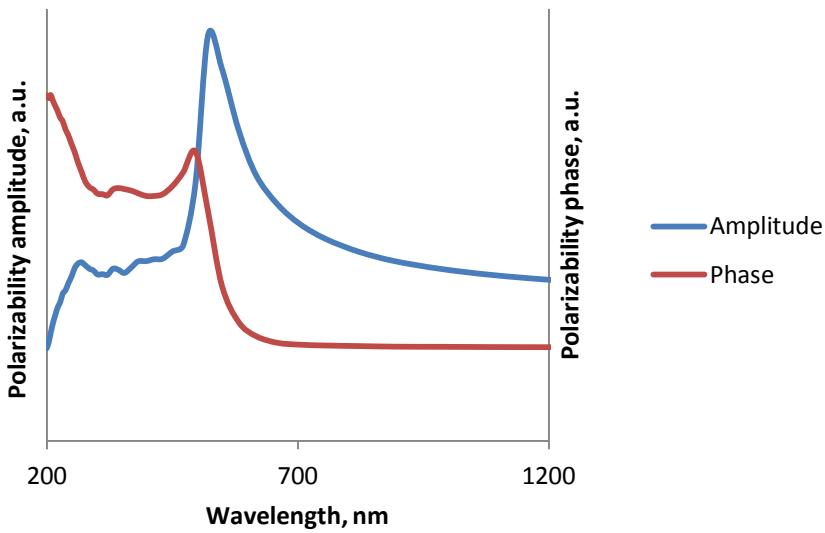

Figure 2.1Amplitude and phase (in arbitrary units) of the polarizability of a small gold nanosphere in vacuum. Dielectric function is given by Johnson and Christy.[42] Here the LSPR occurs at approximately 520 nm.

The quasi static approximation catches essential optical properties of small metallic particles like the fact that their polarizability has a resonant behavior and that the spectral position of this resonance depends on the dielectric functions of both the particle and its environment. It misses, however, important features that become apparent when the optical properties of particles with different shapes and sizes are compared. These features can be elucidated by extending the quasi static approximation to arbitrary spheroids with three principal axes[46] and further by considering radiation damping and dynamic depolarization due to increased size[45, 47, 48].

A more general solution to the quasi static approximation is obtained by solving the Laplace equation in elliptical coordinates:[46]

$$\alpha_i = 4\pi a_1 a_2 a_3 \frac{\varepsilon_l - \varepsilon_m}{3\varepsilon_m + 3L_i(\varepsilon_l - \varepsilon_m)} \tag{2.24}$$

$$L_i = \frac{a_1 a_2 a_3}{2} \int_0^\infty \frac{dq}{(a_i^2 + q) f(q)} \tag{2.25}$$

$$f(q) = \sqrt{(q + a_1^2)(q + a_2^2)(q + a_3^2)} \tag{2.26}$$

$$\sum L_i = 1 \tag{2.27}$$

Here a_1, a_2 and a_3 correspond to the principal half-axes and the polarizability α_i corresponds to the polarization of the particle when the external electric field is directed parallel to any of the axes. This expression is equal to (*2.22*) when the three principal axes are equally long.

This model is useful for modelling the nanodisks or nanoellipses geometries. The different shapes are shown in Figure 2.2. In the case of a nanodisk two principal axes are chosen to be equally long and the third is considerably smaller. The external field is parallel to either of the two longer axes. In this way the nanodisk is modelled as an oblate spheroid. Still, this model is only valid when the particles are much smaller than the wavelength of light.

Radiation damping and dynamic depolarization are effects that gain influence with increasing particle size. Within the framework of electrodynamics radiation damping is treated as the work that the radiation field exerts on the polarized particle. The dynamic depolarization is a result from the integral contribution of each infinitesimal volume element of the particle to the polarization of the center part of the particle. For large particles phase shifts in polarization due to the

dynamics of the radiation will cause the polarization to decrease and spectrally broaden and redshift.[47, 48]

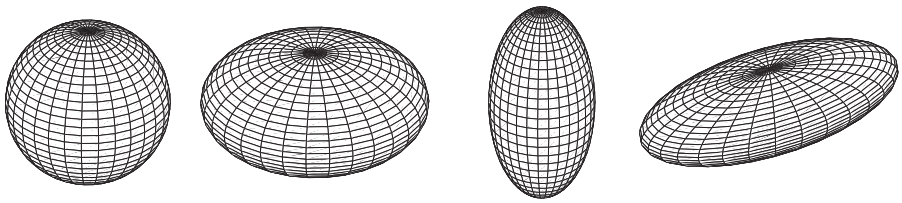

Figure 2.2 Spheroids of different proportions. Left to right: Sphere – all principle axes are equal. Oblate spheroid – two axes are equal and one axis is shorter. This is a simplified nanodisk. Prolate spheroid – two axes are equal and one axis is longer. Ellipsoid – All three principal axes have different lengths. This is a simplified nanoellipse.

The modified long wavelength approximation (MLWA) takes these effects into account. Using the MLWA the quasi-static polarizability is first calculated for the specific geometry. Then the contributions from radiation damping and dynamic depolarization are obtained by integration over the particle volume. Hereby a perturbing factor is obtained that can be inserted into equation (*2.21*) to obtain a correct polarization. For an oblate spheroid being polarized in the plane of the two major axes this factor is given by:[45]

$$F = \frac{1}{1 - \frac{2}{3} ik^3 \alpha - \frac{k^2}{b} \alpha} \qquad (2.28)$$

Here k is the wave number of the external field, α is the polarizability as obtained from the quasi-static approximation and b is the major axes.

If analyzed, the models presented here reveal some rules of thumb regarding the spectral positions of the plasmonic resonances depending on size and shape of the particles. These rules apply if the particles are excited by an electromagnetic field impinging on the top of the particles as they are indicated in Figure 2.2. Larger particles and oblate particles will have resonances shifted to longer wavelengths. Smaller particles and prolate particles will have resonances shifted to shorter wavelengths.

Optical cross-sections

Optical cross-section, σ, is a physical quantity that relates to the tendency of a particle to interact with light. Experimental results obtained from optical spectroscopy are often directly proportional to the optical cross-sections. Individual

cross-sections can be attributed to extinction, scattering and absorption and they are related through the expression:[46]

$$\sigma_{ext} = \sigma_{sca} + \sigma_{abs} \qquad (2.29)$$

In general, (elastic) scattering denotes the changing of light propagation direction due to interactions with the particle and absorption denotes transformation of light into other forms of energy upon interaction with the particle. Extinction is then corresponding to light that deviates from a straight line of propagation past the particle.

The physical dimension of optical cross-sections is area. In a not very physical, but quite intuitive, way of regarding the cross-sections, the light is treated as infinitesimal particles or rays travelling along straight trajectories. The cross-section is then the size of the particle projected onto a plane perpendicular to the light path. The larger the particle is the more light hits it. (In reality, however, the lateral physical dimensions of the particle has little to do with its optical cross-section)

A surface with homogeneously distributed identical nanoparticles provides a good example to illustrate the quantitative nature of optical cross sections. Say that the number density of the particles on this surface is 1 μm^{-2}, 25% of the light intensity impinging on the surface is scattered and 50% is absorbed. Then the scattering and absorption cross sections of each of these identical particles are 0.25 μm^2 and 0.5 μm^2 respectively. This example is valid for arrays of particles on surfaces. For particles in suspension the Beer-Lambert law correlates the cross-sections to light attenuation.[4]

Sometimes the optical cross-sections are normalized to the physical extension of the particle. In that case the resulting ratios are called efficiencies. These efficiencies can have values larger than unity[46], once again proving that optical cross-section have little to do with the physical dimensions of nanoparticles.

2.2 Optical heating of plasmonic metal nanoparticles

Whenever light is absorbed by a plasmonic metal nanoparticle the energy carried by the light is irreversibly transformed via localized surface plasmons into other forms of energy within the nanoparticle. This transformation of localized surface plasmon energy is a multistep process including several branches. This work focuses on the branches generating heat within the particles, other paths will only be mentioned briefly.

The radiative decay path (scattering) is the way for the plasmon to decay without transferring energy to the plasmonic particle itself by instead emitting a photon.

The radiative decay paths are accessible as long as plasmon oscillations are coherent.

Dynamics of non-radiative plasmon decay

Localized surface plasmons are the coherent collective oscillations of the conduction electrons of a metal particle excited by the coupling of a photon to matter. The dynamics of such oscillations can be treated in terms of dephasing time (T_2) and energy relaxation time (T_1).[49] Dephasing times can be experimentally determined either by extinction linewidth measurements[50] or by degenerate four wave mixing (DFWM).[51] Energy relaxation times are determined using femtosecond pump probe experiments.[51]

Typical dephasing times of plasmons in nanoparticles are less than 10 fs but the energy relaxation time is much longer, typically on the picosecond scale.[52] The energy relaxation time is proportional to the intensity of the exciting light while the dephasing time is not.[51]

Dephasing can occur via two main processes; radiative and non-radiative. Scattering corresponding to re-emission of a photon having the same energy as the original photon[4] and near field energy transfer[53, 54] being a mechanism where the plasmon causes excitations in a nearby molecule or semiconductor are both examples of radiative dephasing processes. – They do not cause heating of the particle.

Non-radiative dephasing occurs through the excitation of single electrons through a Landau-type process which causes an athermal electronic distribution.[52] The electrons eventually thermalize through electron-electron scattering. Chemical interface scattering[55] and hot electron enhanced catalytic reactions[56] are the alternative decay paths at this stage.

Electron-phonon scattering is the process by which the particle lattice increases its temperature.[52] It is during this process the particles establish their local temperature. Finally, during particle-environment energy exchange the particle reaches an equilibrium temperature with its surroundings.[52] Thermal equilibrium with the environment can take several nanoseconds to reach.[57]

Local and environmental temperature

Local temperature of and around a plasmonic metal nanoparticle can be calculated using the normal heat-equation, given that no phase transformations occur.[58] Calculations have been made for different conditions involving illumination with continuous and pulsed monochromatic light.[57, 58] In these cases the environment is an infinite thermal reservoir and so only the temperature of the particles themselves and their immediate environment is affected by the illumination. The reservoir itself does not change its temperature.

Efforts to measure the temperature locally around plasmonic particles have also been made. Experiments have involved fluorescence polarization anisotropy, [59, 60] melting of the particles, [43] plasmonic resonance shift due to temperature mediated refractive index change in host matrix [61] and measurement of the thermal expansion of the nanoparticles[62]. These measurements consider the temperature of the particles or their immediate environments. However, the thermal reservoirs are not infinite and could possibly change temperature during measurements.

Figure 2.3 demonstrates the effect of local temperature on nano particles made of nickel. Such temperature increases in combination with the strong size- and shape dependent plasmonic resonance frequency have been utilized in schemes to narrow the size distributions of supported metal nanoparticles.[63]

In comparison to the irradiances considered in the investigations above, i.e. focused laser beams, the solar irradiance of approximately 1 kWm^{-2} [64] is vanishingly small. In addition, its spectral width exceeds that of most plasmonic resonances, whereupon only a fraction of the irradiance can potentially couple to plasmons. Extrapolating the results obtained in the aforementioned calculations to solar irradiances gives very modest, if any, temperature gradients between particles and environment.

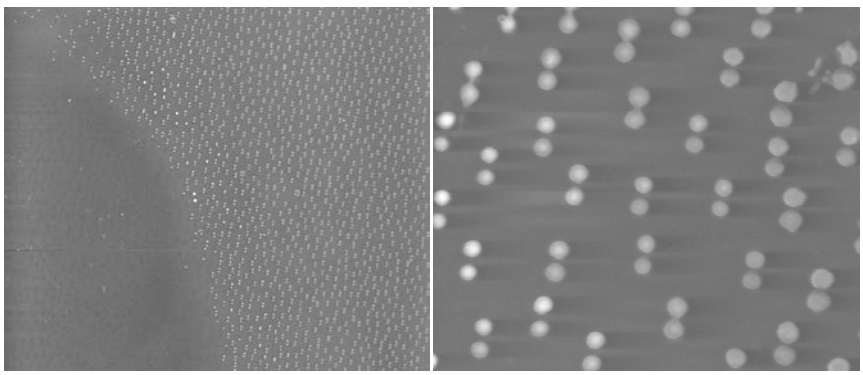

Figure 2.3 Demonstration of pairs of nanodisks composed of Ni that have been illuminated by a 9 µJ nanosecond pulse of 620 nm light. The spatial irradiance profile of the pulse spot is approximately Gaussian. In the center of the spot the high irradiance resulted in the evaporation of the nanoparticles (shown in the left pane). The intensity gradient on the slope of the Gaussian is visible as within a very narrow range the particles have melted without evaporating and outside that range they appear unaffected (right pane).

However, a finite reservoir should eventually experience a temperature increase even at low irradiances and the lack of temperature gradients. Such temperature

increases could be measured even with relatively simple methods. This is discussed further in section 3.4.

2.3 Blackbody radiation

Objects with nonzero temperature emit electromagnetic radiation called thermal radiation or blackbody radiation. A perfect black object radiates according to Planck's law.

$$B_\lambda(\lambda, T) = \frac{2hc^2}{\lambda^5} \frac{1}{e^{\frac{hc}{\lambda k_B T}} - 1} \qquad (2.30)$$

Two major traits of thermal radiation are that the emitted intensity increases with increasing temperature and that the wavelength of the spectral maxima shifts to shorter wavelengths with increasing temperatures.

Very few objects are in fact perfectly black, i.e. absorbing all incoming electromagnetic radiation. Hence the concepts of grey bodies and emissivity emerge. Emissivity, ε, is a material-specific factor between 0 and 1 that is multiplied by Plank's law to determine how much a body radiates. The emissivity of an object is the same as its absorption. Just as absorption, emissivity varies with the wavelength but often it is averaged out to a constant value over a relevant wavelength range. Figure 2.4 shows the spectral profile of blackbody radiation from three objects with different temperature and emissivity.

Glass typically has an emissivity of 0.92. Metals on the other hand typically have low emissivity, close to zero.[65]

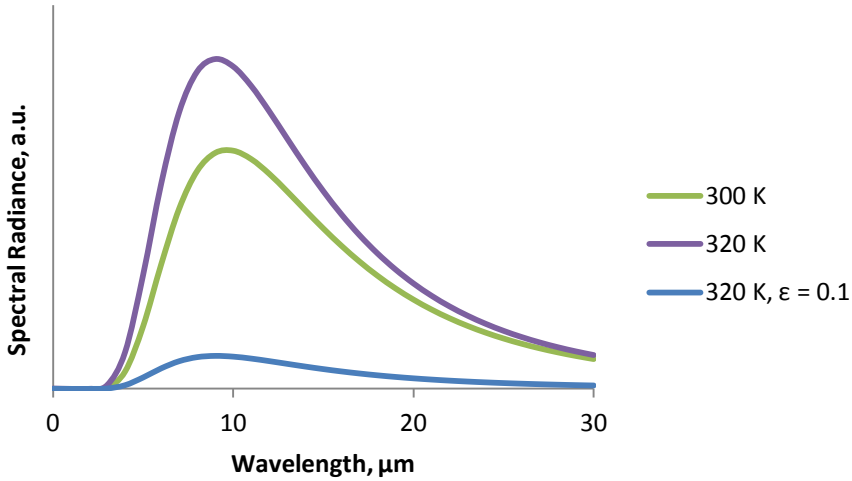

Figure 2.4 Showing spectral profile of blackbody radiation from two perfect black bodies with temperatures of 300 and 320 K respectively. Also included is the spectral profile of a grey body with emissivity 0.1 and temperature of 320K.

3 The Nuts and Bolts

3.1 Hole-mask Colloidal Lithography

Hole-mask Colloidal Lithography (HCL) is a process for fabrication of two-dimensional amorphous arrays of an exceedingly broad range of nanostructures by deposition of material through a metal mask with nanoholes.[66] The nanostructures include nanodisks, nanocones, nanoellipses, nanorings, various composite structures (dimers, trimers, stacks) and many more. The plasmonic structures in this thesis have been fabricated exclusively using the HCL process.

HCL makes use of dispersed polystyrene beads (colloids) to define the pattern of the metal mask with nanoholes. This holes mask rests on a sacrificial layer that, in turn, rests on the substrate intended for the final nanoparticles. The sacrificial layer serves two purposes. First, dissolution of the sacrificial layer permanently removes it and the holes mask. Secondly, it is a mean to offset the mask from the substrate. This offset is a benefit that allows spatial freedom in the exact position of the final nanostructures.

In pH neutral solution the colloids used in HCL typically have negative surface charge (as supplied by the chemical synthesis), thus they repel each other but are attracted to surfaces with positive surface charge. For this purpose a layer of polydiallyldimethylammonium (PDDA), which has a positive charge in neutral pH, is pre-deposited on the surface to be patterned. The colloids stick to the oppositely charged PDDA surface and simultaneously repel each other and so arrange themselves with a well-defined nearest neighbor distance but otherwise without any long-range ordering. Figure 3.1 shows colloids distributed on the surface.

The colloids on the surface shadow discrete surface areas when an etch mask is subsequently deposited on the sample. Due to the relatively weak electrostatic interaction between the colloids and the surface they are easily removed by e.g. adhesive tape or a wet/dry cloth after the etch mask has been deposited. When the colloids have been removed, the etch mask have holes in the place of colloids, C.f. Figure 3.1.

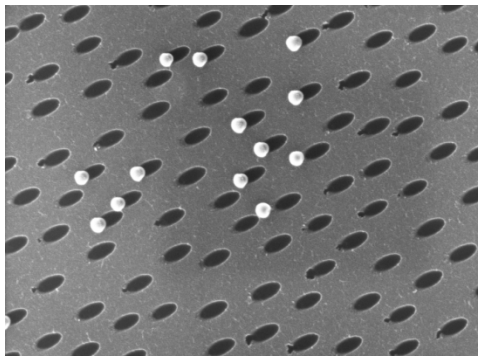

Figure 3.1 Residual colloids lingering on a metal mask with elliptical nanoholes. Some colloids failed to come off during the colloid removal step of HCL. The elliptical holes tell that the hole-mask has been evaporated at an angle.

Plasma etching removes the sacrificial layer locally beneath the holes and establishes a line of sight between the hole-mask and the bottom substrate. The hole-mask now allows area selective materials deposition, preferably by thermal evaporation, onto the substrate. Nano-stacks are possible to deposit through sequential evaporation of different materials. Figure 3.2 illustrates the HCL process in whole.

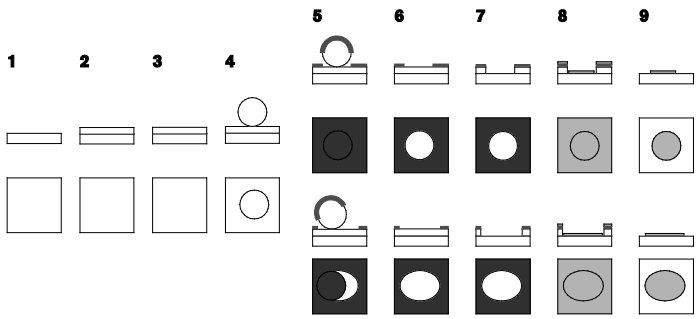

Figure 3.2 Schematic drawing of the HCL sequence. Cross-sectional views and surface normal views of circularly and elliptically shaped nanoholes are presented. 1) The process starts with a clean substrate. 2) Deposition of a sacrificial layer. 3) Drop casting of a PDDA layer (thin) to make sure the surface is positively charged. 4) Positioning of colloids. 5) Evaporation of the metal mask (evaporation at an angle from surface normal results in elliptical holes) 6) Removal of colloids. 7) Plasma etching of sacrificial layer. 8) Deposition of nanostructures. 9) Removal of sacrificial layer and hole-mask.

Choice of Materials and Variations of HCL

Fabrication of some structures and involving some materials require modifications of the HCL process. Evaporation of carbon is one example that can be problematic due to the immense amount of thermal radiation emitted during evaporation. This radiation heats up the sample causing Poly(methyl methacrylate) (PMMA), which is commonly used for sacrificial layer, to melt. Melting the sacrificial layer is totally detrimental to further evaporation of nanostructures through the hole-mask. However, several approaches circumvent this problem.

One approach involves changing the material used for sacrificial layer. The main property of a sacrificial layer is that it dissolves in some agent that doesn't affect the nanostructures or the substrate. Polymers are often used for this purpose as they dissolve in organic solvents while the nanostructures and substrates, usually consisting of metals and oxides, does not. Polysulfone is a polymer that has a higher melting point than PMMA and can thus be used when evaporating carbon. Another possibility is to use some metal for the sacrificial layer. Metals can be chemically etched by acids and the issue then reduces to finding an etching agent that only removes the sacrificial layer.

Changing the sacrificial layer to a metal might also require a change of material for the hole-mask as this must have considerably lower dry etch rate than the sacrificial layer. The choice of sacrificial layer dictates which process is used for dry etching. From there a suitable material can be chosen for the hole-mask.

A second approach is to deposit carbon, or any other material that cannot be evaporated through a hole-mask, as a continuous film. HCL can then be used to deposit material that locally protects areas of the film from later etching or ion-milling. This etching or ion-milling removes the film material not covered by the protecting HCL structure. Multilayered structures can also be fabricated by this method simply by evaporating several continuous film layers before doing HCL. A version of this approach is used in paper 4 of this thesis.

3.2 Techniques for Adding and Removing Material on the Nanoscale

Spin-Coating

Spin coating is a technique for coating substrate surfaces with thin films from liquid solutions. Deposition is done by placing the substrate to be coated on a rotatable holder, a spinner. The coating solution is applied on the sample surface whereupon holder and sample is spun for a given period of time. The apparent centrifugal force causes the solution to flow off the substrate and the liquid film thickness reduces. For each angular speed the residual film thickness will converge to some solution specific value. In order to improve the quality of the film, specifically its homogeneity, adapted acceleration rates and sequences of different

angular speeds may be employed. Many spinners may be programmed to execute this automatically.

E-beam assisted thermal evaporation

E-beam assisted thermal evaporation is an *in vacuo* method to deposit thin films of material from solid state sources onto substrates. In principle, a filament, shielded from the material source, emits electrons, usually thermionically. An electrostatic filed accelerate the emitted electrons by several kV while a magnetic field focus them on the source. The electron current heats the source material until it starts to vaporize. Due to the low gas pressure inside the process chamber the vapor species travel with molecular flow, meaning that their mean free paths are longer than the dimensions of the chamber. At high evaporation rates the evaporated species form a viscous region above the source. In this case a virtual source is positioned slightly above the real source. Because both virtual and real source are small and the gas travels with molecular flow .i.e. straight lines, clear shadow effects arise making this technique highly suitable for material deposition through HCL masks [67].

Plasma etch

Plasma etching is a method for removing atoms from a sample by immersing the sample into a plasma. A plasma is an ionized gas with zero net charge consisting of ions, electrons and neutral atoms and molecules. Plasma etching removes material by two main mechanisms. Ions that are accelerated towards the sample by means of an electric field may, by pure kinetic energy, knock out material from the sample. This is known as sputter etching. Alternatively, chemically reactive gas-phase species within the plasma undergo reactions with the sample material and form volatile products. This is known as chemical etching. Masks, made from materials with low etch-rates, render area selective etching when they are placed on the material to be etched.[67]

Sputtering

Sputtering is a method to deposit thin films on substrates from solid sources. Sputter sources are called targets and they have to be electrically conducting. The sputter process takes place a controlled low pressure atmosphere. Control is achieved by evacuating the chamber before process and then partially filling it with a gas that will be ionized during evaporation. Typical process gases are the noble gases: Argon, Krypton and Xenon. The target is negatively biased and attracts positive ions from the ionized gas. When the ions impact the target they transfer kinetic energy that makes other atoms leave the target. These atoms eventually condense on the substrate and form a film. In sputtering the target is rather large, typically having the same dimensions as the area being coated. Species leaves the target at a wide solid angular distribution and so there is relatively little shadow

effects. This makes it possible to coat topological samples but impossible to deposit nanostructures through an HCL mask.

Reactive sputtering is a sputter process that facilitates sputtering of carbides, oxides and nitrides by adding a reactive gas into the process chamber. The gas prompts a chemical reaction with the element of the target and the resulting compound species are sputtered instead of the pristine target material.[68]

3.3 Materials Characterization

This section mainly deals with the different techniques used to assess samples with respect to various physical properties.

Scanning Electron Microscopy

Structural characterization of supported metal nanoparticles generally concerns their size, shape and areal number density. These properties, except from particle height, are readily assessable via Scanning Electron Microscope, SEM. For characterization of particles supported by an electrical insulator Environmental SEM, ESEM, is used instead. The general working principles are similar for both kinds of microscopes.

SEM, in general, forms images, micrographs, by scanning a probing beam of electrons across the sample in a low pressure environment. The beam typically consists of 5 to 20 keV electrons and is focused on a spot less than 5 nm in diameter on the sample surface. Signal is obtained from detecting electrons emitted from the illuminated spot. Two imaging modes stem from the detection of secondary electrons, SE, and backscattered electrons, BSE, respectively. [69]

Secondary electrons have low energy and are residuals from the ionization of the sample by the probing beam. These electrons have a short mean free path within the sample. Consequently only species originating from a thin layer below the surface escape into the vacuum and are possible to detect. Contrast is given by the angle of incidence of the probing beam and the secondary electron yield of the material. This in combination with the surface bound origin of the electrons make secondary electron imaging suitable for topological studies. The resolution of micrographs from secondary electrons is often better than 10 nm. [69]

Backscattered electrons have energies identical to, or slightly lower than, the probing beam. They have longer mean free paths and consequently probe deeper into the sample than the secondary electrons. Contrast arises from the angle of incident beam to sample surface normal and from the atomic number of the sample material. This makes backscattered electrons useful for compositional analysis as well as topological.

As SEM involves shooting an electron beam on the sample, the sample needs to be electrically conducting in order to carry away excess charge. In the case of poorly conducting samples charges needs to be carried away by some other means. ESEM is designed to operate at higher sample compartment pressures and therefore allows excess charge to be carried away by ionized gas species [70].

The higher pressure of the ESEM has consequences for imaging. Increased pressure leads to shorter mean free paths of electrons. For the probing beam the shorter mean free path leads to electrons being scattered and removed from the focused beam. The beam does not broaden by the scattering but it becomes less intense and the scattered electrons contribute to background noise. As a result the spatial resolution does not change but the contrast may deteriorate. [70]

Due to the high energy of backscattered electrons they are still possible to detect at high pressures with the same apparatus as for high vacuum SEM. Secondary electrons, on the other hand, are impossible to detect using the same sort of detectors. Instead advantage is taken by the fact that the emitted electrons ionize the chamber gas. The detection of ionized gas species may even lead to an enhancement of the signal as avalanche ionization of the gas is possible to achieve with an electrical bias. [70]

Quartz Crystal Microbalance with Dissipation Monitoring

Quartz crystals pose excellent voltage-driven mechanical oscillators with low intrinsic losses and highly resolvable resonance frequencies. By virtue of a well-defined relationship, laid out by the Sauerbrey equation, shifts in resonance frequency can be strictly related to the mass of rigid material added onto quartz crystals. As a result quartz crystals are widely used as microbalances in vacuum, gas and liquid.[71]

However, in liquid the Sauerbrey equation only holds for thin, non-porous and evenly distributed films. Otherwise oscillating energy dissipates through couplings between the added material and the liquid which cause the result to become ambiguous. [71]

To circumvent this problem the quartz crystals can be driven intermittently whereupon both resonance frequency and dissipation can be measured simultaneously via the ring-down of the crystal oscillation. This setup goes under the name Quartz Crystal Microbalance with Dissipation Monitoring (QCM-D).

QCM-D is a highly suitable technique for studying sorption mechanisms involving biomaterials in aqueous solution as it gives information on both mass and viscoelasticity.[72]

Optical Spectroscopy

Optical extinction-, absorption- and scattering cross-sections are often measured with a spectrophotometer. The kind of spectrophotometer used in this thesis uses a monochromator to illuminate a sample one wavelength at a time. Depending on which mode the instrument operates in only transmitted or transmitted plus scattered light intensities may be collected. Figure 3.3 shows the principles of the two modes. The collected light intensities are compared to a reference measurement to extract information about the optical cross-sections.

Supported nanoparticles strongly interact with the substrate and the reference measurement should correspond to an empty sample compartment. In this way the combined optical cross-sections for glass and particles are considered.

In the case of collected transmitted light the collected light intensities from sample divided by the collected light intensities from reference and subtracted from unity is proportional to the extinction cross-section. When instead transmitted plus scattered light is collected the same expression is proportional to the absorption cross-section. The scattering cross-section may be calculated from the optical theorem which states that the scattering cross-section equals the extinction cross-section minus the absorption cross-section [46].

The method described above is not sufficient to quantify the cross-sections of individual supported plasmonic metal nano-particles. Assuming that the particles covering a sample are homogeneous in size, shape and material composition, the dimensionless quantities obtained as above must also be divided by the areal number density of the particles. In this way quantities with area dimensionality are obtained. The cross-section area is an abstract construction that denotes the area perpendicular to light incidence required by each particle to geometrically intercept the proportion of light rays that are removed in measurement.

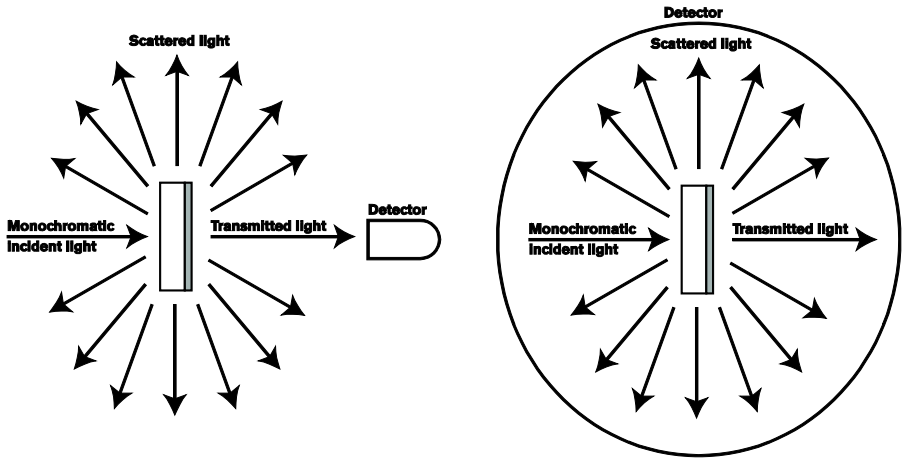

Figure 3.3 Schematic drawings of the two principal measurement modes for optical spectroscopy. The left drawing illustrates transmission measurements. Here the detector only collects light that travel in a straight line through the sample. The right drawing illustrates transmission + scattering measurements. In this case the detector collects both transmitted and scattered light.

In this thesis the cross-sections are not quantified for individual particles, instead the non-normalized cross-sections are used and in particular the absorption. The information given by this measure is then the wavelength resolved fraction of irradiance that is absorbed by the sample. Given that the irradiance from a light source is known the total absorbed power can readily be calculated by multiplying the two spectra wavelength by wavelength and integrating. This calculated absorbed power can later be compared to the measured generated heat.

Thermal imaging

Different types of thermal imaging systems exist. The system used in this thesis is based on a non-cooled microbolometer array sensitive in the wavelength range 7.5 to 13 μm [73]. A bolometric detector is in principle a resistor with small heat capacity and a negative temperature coefficient of resistivity [65]. The resistor is covered with an infrared absorbing film and reports a temperature increase that is proportional to the amount of absorbed radiation. A thermal imaging system comprises an array of micrometer-sized bolometers that is placed in the image plane of an infrared lens. Hereby they produce 'images' of the sensed infrared intensity. Such images are often called thermograms.

Microbolometer arrays lack spectral resolution. The temperature is determined on the basis of total absorbed power in the sensitive wavelength range according to a camera internal algorithm. The exact algorithm is undisclosed[65], but takes into

consideration user-specified values for object emissivity, object-camera distance, ambient temperature, atmospheric temperature and atmospheric relative humidity.

Emissivity is a central concept in thermal imaging. The ideal amount of power radiated by an object is determined by Planck's law. That law is valid if the radiating object is a perfect absorber, i.e. a black body. Real materials are rarely black bodies; instead their absorbance varies with the wavelength of light. Bodies with a wavelength invariant absorbance are called grey bodies. The amount of power radiated from a grey body is a fraction of the ideal black body radiation. This is compensated for in Plank's law with a factor denoted emissivity having a value between 0 and 1.

Ambient temperature affects the measurements as thermal radiation emitted from the surrounding environment, i.e. walls and the ground, is reflected by the imaged object and thereby adds to the reading. Object to camera distance, atmospheric temperature, and relative humidity plays a role as the atmosphere both absorbs the radiation from the object and also emits radiation by itself. For camera-to-object distances closer than one meter atmospheric influences are very small in the 7.5 to 13μm wavelength band.

Calibration of the thermal camera is usually done by assigning the object to be imaged with a specific emissivity [65]. In practice this is achieved by measuring the temperature of a surface both with a thermocouple and with the thermal camera at some temperature elevated by some tens of degrees above the ambient. The user specified emissivity value of the object is then adjusted until the camera reports a temperature matching that of the thermocouple.

Atomic Force Microscopy

The Atomic Force Microscope (AFM) is, conceptually, a simple instrument for probing surface topologies at high resolution in atmosphere or liquid. A very sharp tip scans the surface and does the actual probing of the topology. The tip is situated on a cantilever that bends when the tip experiences attractive or repulsive forces from the surface. A laser beam is reflected off the cantilever onto a position sensitive photo detector. Bending of the cantilever causes the laser beam to be reflected onto a different position on the photodetector. In this way the photo detector reports what forces the probing tip experiences. Piezo-electric crystals move the tip in three dimensions. Final resolution is often limited by the sharpness of the probing tip.[74]

3.4 Measuring temperature of plasmonic particle environment under solar illumination

In this thesis temperatures of supported nanoparticles were measured under direct solar illumination. As was discussed previously those conditions does not imply

any temperature gradient between particle and support. In practice that means that substrate temperature equals particle temperature and that the two can be measured interchangeably. Figure 3.4 illustrates experimental setup for measuring the temperature of plasmonic particle decorated glass samples under solar illumination. In principle temperature increases due to optical absorption can be measured by this setup for any type of absorbing film.

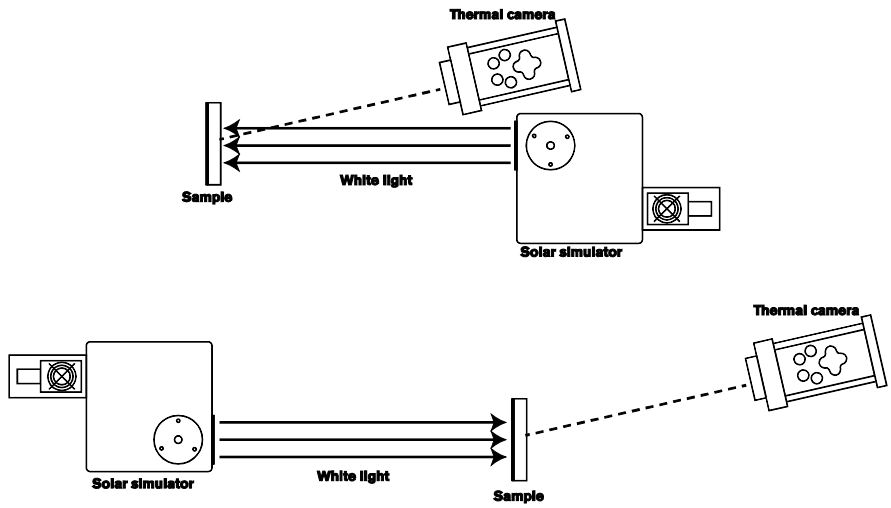

Figure 3.4 Thermal measurement setup. Top sketch illustrates the setup when light source is illuminating the pristine sample surface. Bottom sketch illustrates the setup when the decorated sample surface is illuminated. The thermal camera images the pristine surface in both setups. The different parts of the setups are not drawn to scale.

A solar simulator, the sample and a thermal camera constitutes the setup. The sample can be oriented with either surface, pristine or decorated, facing the light source. The thermal camera has to image the pristine surface: The solar absorbing surface could affect the emissivity of the surface and add uncertainty to the measurement. The pristine surfaces of samples are also conformable when the absorbing surfaces are dissimilar, thus isolating any differences in results to the absorptive properties.

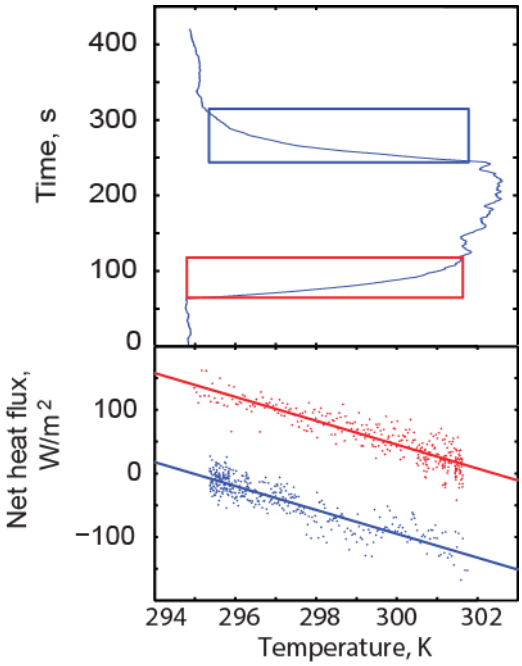

Figure 3.5 Graphs illustrating the temperature of a sample during a light on - light off cycle and the derived heat fluxes. Top graph, time on vertical axis and temperature on horizontal, shows the temperature dynamics of a sample that is initially kept in dark. At 60 s solar light is instantaneously turned on and at 240 s it is instantaneously turned off. The red and blue areas mark two sets of data-points that correspond to the light-on and light off responses respectively. The bottom graph shows the temporal derivative of the two temperature responses multiplied with the thermal mass of the sample (vertical axis) plotted against the temperature (horizontal axis). Solid lines are linear fits to the two data sets. The vertical difference between these two lines corresponds to the absorbed irradiance.

The setup is used to subject samples to a light on - light off cycle and track their resulting temperature responses. Figure 3.5 shows the temperature profile of a sample and the result of post processing.

Here, post processing relies on the establishment of a thermal equilibrium between the sample and its environment and that the environment has a constant temperature. The heat transfer mechanisms that govern this equilibrium are convection and thermal radiation. The amount of heat exchanged by convection is regarded to be directly proportional to the temperature difference between sample and environment while the amount exchanged by thermal radiation is regarded to be proportional to the difference between the fourth powers of the sample and environment temperatures. [75] As the temperature difference (in this case) is small in

relation to the absolute temperature, also the contribution from radiation can be regarded to be linear.

Optical absorption shifts the equilibrium temperature of the sample when the light source starts to illuminate it. Heat begins to flow from the sample to the environment at the rate determined by the approximately linear relation between sample and environment temperatures determined for convection and thermal radiation. A new equilibrium temperature is reached when thermal radiation and convection release as much heat as optical absorption adds. Conversely, the sample returns to room temperature at a rate determined by its momentary temperature when illumination ends.

Actual heat flow can be extracted from the time-resolved temperature measurements of the sample. A change in sample temperature corresponds to a change in its thermal energy as specified by the thermal mass of the sample. Since the thermal mass of the sample is known from material data, the change in energy and consequently heat flow is readily calculated.

The difference in heat flow, at any sample temperature, between the light-on and light-off data sets simply correlates to the heat added by optical absorption. This method provides an alternative way to determine optical absorption and at the same time provides insight into the correlating temperature effects.

4 Summary of Appended Papers

4.1 Paper 1 – Graphene Oxide and Lipid Membranes: Interactions and nanocomposite structures

This paper is a study on the basic interactions between lipid membranes and suspensions of graphene oxide (GO) flakes (0.5 – 5 μm in size). Real time observations of interactions are made independently by QCM-D and DPI. Sample surface topography is post-studied by AFM.

GO has negative ζ-potential and is expected to be attracted by positive ζ-potentials. Exposing supported lipid bilayers having either positive or negative ζ-potentials depending on lipid composition to GO suspension shows that GO is taken up by lipid membranes having positive ζ-potential but not by membranes having negative ζ-potential. The GO binds flatly to the lipid membranes with both gaps between the GO flakes and overlaps.

Alternating exposure of GO suspension and positively charged liposomes allows layer-by-layer growth. Exposing a surface of GO flakes bound to a lipid bilayer to liposomes will cause the liposomes to adhere to the GO flakes but not to rupture. Subsequent exposition to GO-flakes will induce rupture of the liposomes and formation of multilayer stacks. These stacks remain intact even after sample drying.

4.2 Paper 2 – Nanplasmon-enabled thermal management

This paper compares the light-to-heat conversion efficiency of the surfaces comprising the amorphous arrays of nanodisks or nanoellipses of Au or Ni. The surfaces are fabricated on transparent glass substrates using HCL. The paper furthermore presents a method to measure the thermal energy, generated by these surfaces, in units of power per area. This method relies on the time resolved thermal imaging of the substrate under the light on/light of cycle. The light source in this paper is a solar simulator of AM1.5G solar light.

Conversion efficiency is estimated both by the integration of optical absorption spectra and by the thermal imaging. Plasmonic particles of Au and Ni have qualitatively different optical responses following their respective material properties. For the single wavelength absorption Au would obviously be the best materials choice having strong peak absorption. For the broadband absorption of solar light, however, Ni has the highest heat conversion efficiency of the two.

4.3 Paper 3 – Solar transparent radiator using optical antennas

Paper 3 merges the conclusions from paper 2 with the antenna designs used in the previous work by Tong et. al.[76] These antenna designs comprise multiple plasmonic elements and dielectric spacer elements in a stack configuration.

Such nanoantennas built from the circular nanodisks of Au spaced by silica (SiO_2) or alumina (Al_2O_3) show strong dependence of the light-to-thermal energy conversion efficiency on the direction of light propagation. Nanoantennas of a single plasmonic element are more efficient in heat conversion of light that is incident on the antennas from the transparent substrate side. Adding more Au elements to the nanoantenna and forming a vertical stack reverses this behavior and the nanoantenna of three Au elements becomes a more efficient converter of light incident from the air side. Furthermore, spectral broadening of the optical response as a consequence of added plasmonic elements with mutually offset resonance frequencies contributes to the overall increase in light-to-heat conversion efficiency of the solar light.

Changing the geometries of the antennas and switching to lossy materials, analogously to paper 2, doubles the conversion efficiency. However, further addition of the plasmonic elements to the nanoantenna stacks doesn't improve the conversion efficiency considerably.

These surfaces have potential use as window coatings for the increased indoor thermal comfort. As such, their optical filtering the incident light is critical. Quality of the transmitted (illuminating) light is often determined by assigning a color rendering index. Due their smooth and broad optical spectra these coatings provide excellent color rendering up to 98%.

4.4 Paper 4 - Absorbing nanoplasmonics with naturally abundant materials for solar energy harvesting

This paper studies the materials that by themselves have a modest set of properties as plasmon resonators or absorbers, but combined in nanoantennas deliver superior

ability to convert solar light into thermal energy while keeping the transparency of the supporting material.

Specifically the naturally abundant materials Al, Fe and C are targeted. These materials are interesting from an economical point of view but are relatively unexplored in nanoplasmonics. Here they are employed in the different parts of the plasmonic Yagi-Uda antenna analogues. These elements include a reflector, an absorber (feed) and, optionally, a director. C and Fe are highly optically and electrically lossy materials and are thus very suitable for the use as absorbing elements. Al has relatively strong plasmonic resonances and is suitable for the reflecting and directing elements.

C-Al antennas comprising reflector and absorber are fabricated by HCL on the transparent substrates in two different configurations. The first configuration builds on the inherent property of the supported plasmonic particles to have the higher absorption when illuminated from the transparent support. The positions of the reflector (Al) and absorber (C) are changed to elucidate the effects of the antenna design on the optical absorption.

With the help of FDTD simulations we determine the optimum antenna element separations to reach the most efficient light absorption. The Al-Fe nanoantennas with the reflector, absorber and director elements are the fabricated following the recipes from the electromagnetic simulations. Thus the simulations are experimentally validated and high optical absorptions are reached with these nanoantennas.

The results point out that absorption is indeed enhanced by these antenna geometries, further producing sizeable directionality in absorption.

5 Conclusions and Outlook

Results from paper 1 point at a new fabrication method to form composite structures with GO intercalated between lipid membranes. Exactly where these structures find application poses an open question to be answered in the future. As of now the method adds another tool to the nanofabrication toolbox.

In the context of plasmon-assisted light harvesting this work has pointed out a route towards absorptive transparent surfaces. Window coatings for increased indoor thermal comfort pose one possible application for these surfaces.

In order to generate maximize the light-to-thermal energy conversion efficiency of the plasmonic antennas the spectral position of the absorption was set to coincide with the maximum intensity of solar light. This maximum lies in the visible part of the solar spectrum. Naturally, absorption in this region strongly affects the visibility through the coating. A considerable part of the energy of solar light lies in the infrared part of the spectrum. Tuning the absorption spectra of the plasmonic antennas to cover also this part is a possible future undertaking.

One approach to extend the bandwidth of the antennas could be to merge multiple antennas individually tuned to different wavelengths. A compact way of realizing this could be to stack two Yagi-Uda antennas and combine the director element of the bottom, long wavelength, antenna with the reflector element of the top, short wavelength, antenna.

The lateral extensions of the coatings are also a matter of future interest. The areas of samples coated in this thesis are limited to 2 cm^2. Window panes used in contemporary buildings can be four orders of magnitude larger. The fabrication process obviously needs to be adapted in order to allow deposition of plasmonic antennas over such larges surfaces.

Apart from window coatings the Yagi-Uda antenna design could be applied to the local heating of nanoscopic particles. Typically particles with large optical cross sections are used for this purpose. However, with this method even particles with small optical cross sections could be optically heated with relatively low light intensities. This could be of interest in the area of magneto optics.

In general, and that's the beauty of science, you never know to what use results may come. All that can be said with certainty is that a small piece of information has been added to the collective knowledge, free to use by anyone.

Acknowledgements

Writing this book may have been a one-person job, but the work that provides the basis for it has definitely involved the contributions of others.

First of all, nothing of it would have happened without the financial support given by the Swedish Foundation for Strategic Research (SSF) through grants RMA08-0109 and RMA11-0037.

In addition some persons have invested time and effort to help me during this project. Others have been helpful without any effort at all. I hope that I manage to recognize everyone in the following statements.

Mikael Käll has been my boss, examiner and the project leader of both abovementioned research projects.

Alexandre 'Sascha' Dmitriev, my ever optimistic supervisor that's made sure there was a thesis to write.

Dinko Chakarov, also my supervisor and the person that took me on in the first place, seemingly ages ago.

Igor Zoric, my assistant supervisor. Sometimes, knowing there is a door to knock on is as important as the actual knocking. Though, I think I actually did knock a couple of times.

The science was done in collaboration with Bengt Kasemo, Sofia Svedhem, Rickard Frost, Tavakol Pakizeh, Lianming Tong, Vladimir Miljkovic, Manoj Jaysankar, Hans Fredriksson and Raja Sellappan. I especially want to recognize Rickard who taught me everything about lipid membranes and QCM-D, Vladimir who spent time to make numerical models for me when I was figuring out how to extract absorption from temperature responses and finally Manoj, my master-student, who did valuable laboratory work and made me figure out answers to his bright questions.

This work is mainly based on experiments and in order to get experiments to work you need access to working tools and experimental setups. Sometimes you also need someone who knows how to use those tools and setups.

The cleanroom run by MC2 at Chalmers is a marvelous resource for nanofabrication. Much due to the personnel maintaining it. I especially want to recognize the expertise advices and assistance given by Henrik Frederiksen and Mats Hagberg.

During the years I have borrowed a lot of laboratory equipment from others. I am grateful for the generosity of the Chemical Physics Division and especially Christoph Langhammer, Björn Wickman and Mattias Eng.

Also Ingvar Albinsson and Curt Nyberg were generous in letting me use their thermal camera before I got my own.

Then Timur Shegai, Martin Wersäll, Moa Sandberg Wranne and Bo Albinsson helped out with various fluorescence measurements that unfortunately never made it to publication.

Kristina Wettergren, Raja, Beniamino Iandolo, Lars Hellberg, Zhaleh Pirzadeh, Kristof Lodewijks and Ruggero Verre have offered valuable assistance and advice in many practical experimental details.

Apart from experiments there has also been some numerical modelling. Here Tomasz Antosiewicz and Nils Odebo Länk have kindly offered their help.

This work has involved more than mere practicalities. There has been some theoretical discussion going on as well. Robin Ogier and Carl Wadell, in particular, have suffered visits whenever I have had ideas I wanted to vent.

Then, of course, a positive working environment has indeed been helpful. Past and present office mates, Carl Hägglund, Kristina, Anna Clemens, Kristof, Inès Massiot, Irina Zubritskaya and Nicolò Maccaferri have certainly contributed to this. As has past and present members of the divisions of Bionanophotonics, Chemical Physics and Biological Physics.

Finally, my family must be acknowledged for having put up with this.

Bibliography

1. Rao, C. N. R. & Cheetham, A. K. Science and technology of nanomaterials: current status and future prospects. *Journal of Materials Chemistry* **11,** 2887-2894 (2001)
2. Novoselov, K. S., Geim, A. K., Morozov, S. V., Jiang, D., Zhang, Y., Dubonos, S. V., Grigorieva, I. V. & Firsov, A. A. Electric Field Effect in Atomically Thin Carbon Films. *Science* **306,** 666-669 (2004)
3. Geim, A. K. & Novoselov, K. S. The rise of graphene. *Nat Mater* **6,** 183-191 (2007)
4. Kreibig, U. & Vollmer, M. *Optical properties of metal clusters* (Springer, Berlin ; New York, 1995)
5. Alberts, B. *Molecular biology of the cell* 4. edn(Garland Science, New York, 2002)
6. Keller, C. A., Glasmästar, K., Zhdanov, V. P. & Kasemo, B. Formation of Supported Membranes from Vesicles. *Physical Review Letters* **84,** 5443-5446 (2000)
7. Hong, S., Hessler, J. A., Banaszak Holl, M. M., Leroueil, P., Mecke, A. & Orr, B. G. Physical interactions of nanoparticles with biological membranes: The observation of nanoscale hole formation. *Journal of Chemical Health and Safety* **13,** 16-20 (2006)
8. Edvardsson, M., Svedhem, S., Wang, G., Richter, R., Rodahl, M. & Kasemo, B. QCM-D and Reflectometry Instrument: Applications to Supported Lipid Structures and Their Biomolecular Interactions. *Analytical Chemistry* **81,** 349-361 (2009)
9. Dreyer, D. R., Park, S., Bielawski, C. W. & Ruoff, R. S. The chemistry of graphene oxide. *Chemical Society Reviews* **39,** 228-240 (2010)
10. Ang, P. K., Jaiswal, M., Lim, C. H. Y. X., Wang, Y., Sankaran, J., Li, A., Lim, C. T., Wohland, T., Barbaros, Ö. & Loh, K. P. A Bioelectronic Platform Using a Graphene−Lipid Bilayer Interface. *ACS Nano* **4,** 7387-7394 (2010)

11. Ham, M.-H., Choi, J. H., Boghossian, A. A., Jeng, E. S., Graff, R. A., Heller, D. A., Chang, A. C., Mattis, A., Bayburt, T. H., Grinkova, Y. V., Zeiger, A. S., Van Vliet, K. J., Hobbie, E. K., Sligar, S. G., Wraight, C. A. & Strano, M. S. Photoelectrochemical complexes for solar energy conversion that chemically and autonomously regenerate. *Nat Chem* **2,** 929-936 (2010)

12. Sondergaard, T., Novikov, S. M., Holmgaard, T., Eriksen, R. L., Beermann, J., Han, Z. H., Pedersen, K. & Bozhevolnyi, S. I. Plasmonic black gold by adiabatic nanofocusing and absorption of light in ultra-sharp convex grooves. *Nature Communications* **3,** 969 (2012)

13. Aubry, A., Lei, D. Y., Fernandez-Dominguez, A. I., Sonnefraud, Y., Maier, S. A. & Pendry, J. B. Plasmonic Light-Harvesting Devices over the Whole Visible Spectrum. *Nano Letters* **10,** 2574-2579 (2010)

14. Teperik, T. V., de Abajo, F. J. G., Borisov, A. G., Abdelsalam, M., Bartlett, P. N., Sugawara, Y. & Baumberg, J. J. Omnidirectional absorption in nanostructured metal surfaces. *Nature Photonics* **2,** 299-301 (2008)

15. Aydin, K., Ferry, V. E., Briggs, R. M. & Atwater, H. A. Broadband polarization-independent resonant light absorption using ultrathin plasmonic super absorbers. *Nature Communications* **2,** 517 (2011)

16. Cesario, J., Quidant, R., Badenes, G. & Enoch, S. Electromagnetic coupling between a metal nanoparticle grating and a metallic surface. *Optics Letters* **30,** 3404-3406 (2005)

17. Liu, N., Mesch, M., Weiss, T., Hentschel, M. & Giessen, H. Infrared Perfect Absorber and Its Application As Plasmonic Sensor. *Nano Letters* **10,** 2342-2348 (2010)

18. Atwater, H. A. & Polman, A. Plasmonics for improved photovoltaic devices. *Nature Materials* **9,** 205-213 (2010)

19. Moreau, A., Ciraci, C., Mock, J. J., Hill, R. T., Wang, Q., Wiley, B. J., Chilkoti, A. & Smith, D. R. Controlled-reflectance surfaces with film-coupled colloidal nanoantennas. *Nature* **492,** 86-89 (2012)

20. Niesler, F. B. P., Gansel, J. K., Fischbach, S. & Wegener, M. Metamaterial metal-based bolometers. *Applied Physics Letters* **100,** (2012)

21. Liu, X. L., Tyler, T., Starr, T., Starr, A. F., Jokerst, N. M. & Padilla, W. J. Taming the Blackbody with Infrared Metamaterials as Selective Thermal Emitters. *Physical Review Letters* **107,** (2011)

22. Bermel, P., Ghebrebrhan, M., Chan, W., Yeng, Y. X., Araghchini, M., Hamam, R., Marton, C. H., Jensen, K. F., Soljacic, M., Joannopoulos, J. D., Johnson, S. G. & Celanovic, I. Design and global optimization of

high-efficiency thermophotovoltaic systems. *Optics Express* **18,** A314-A334 (2010)

23. Yen, C. W. & El-Sayed, M. A. Plasmonic Field Effect on the Hexacyanoferrate (III)-Thiosulfate Electron Transfer Catalytic Reaction on Gold Nanoparticles: Electromagnetic or Thermal? *Journal of Physical Chemistry C* **113,** 19585-19590 (2009)

24. Neumann, O., Urban, A. S., Day, J., Lal, S., Nordlander, P. & Halas, N. J. Solar Vapor Generation Enabled by Nanoparticles. *ACS Nano* **7,** 42-49 (2012)

25. Polman, A. Solar Steam Nanobubbles. *ACS Nano* **7,** 15-18 (2013)

26. Cao, L., Barsic, D. N., Guichard, A. R. & Brongersma, M. L. Plasmon-assisted local temperature control to pattern individual semiconductor nanowires and carbon nanotubes. *Nano Letters* **7,** 3523-3527 (2007)

27. Boyd, D. A., Greengard, L., Brongersma, M., El-Naggar, M. Y. & Goodwin, D. G. Plasmon-assisted chemical vapor deposition. *Nano Letters* **6,** 2592-2597 (2006)

28. Challener, W. A., Peng, C. B., Itagi, A. V., Karns, D., Peng, W., Peng, Y. Y., Yang, X. M., Zhu, X. B., Gokemeijer, N. J., Hsia, Y. T., Ju, G., Rottmayer, R. E., Seigler, M. A. & Gage, E. C. Heat-assisted magnetic recording by a near-field transducer with efficient optical energy transfer. *Nature Photonics* **3,** 220-224 (2009)

29. Donner, J. S., Baffou, G., McCloskey, D. & Quidant, R. Plasmon-assisted optofluidics. *ACS Nano* **5,** 5457-5462 (2011)

30. Wu, T. H., Teslaa, T., Kalim, S., French, C. T., Moghadam, S., Wall, R., Miller, J. F., Witte, O. N., Teitell, M. A. & Chiou, P. Y. Photothermal nanoblade for large cargo delivery into mammalian cells. *Analytical Chemistry* **83,** 1321-1327 (2011)

31. Zhu, M., Baffou, G., Meyerbroker, N. & Polleux, J. Micropatterning Thermoplasmonic Gold Nanoarrays To Manipulate Cell Adhesion. *ACS Nano* **6,** 7227-7233 (2012)

32. Zhao, W. & Karp, J. M. Tumour targeting: Nanoantennas heat up. *Nature Materials* **8,** 453-454 (2009)

33. Gobin, A. M., Lee, M. H., Halas, N. J., James, W. D., Drezek, R. A. & West, J. L. Near-infrared resonant nanoshells for combined optical imaging and photothermal cancer therapy. *Nano Letters* **7,** 1929-1934 (2007)

34. Jeon, I. T., Cho, M. K., Cho, J. W., An, B. H., Wu, J. H., Kringel, R., Choi, D. S. & Kim, Y. K. Ni-Au core-shell nanowires: synthesis, microstructures, biofunctionalization, and the toxicological effects on

pancreatic cancer cells. *Journal of Materials Chemistry* **21,** 12089-12095 (2011)

35. Jain, P. K., El-Sayed, I. H. & El-Sayed, M. A. Au nanoparticles target cancer. *Nano Today* **2,** 18-29 (2007)

36. Liu, H., Chen, D., Tang, F., Du, G., Li, L., Meng, X., Liang, W., Zhang, Y., Teng, X. & Li, Y. Photothermal therapy of Lewis lung carcinoma in mice using gold nanoshells on carboxylated polystyrene spheres. *Nanotechnology* **19,** 455101 (2008)

37. Lal, S., Clare, S. E. & Halas, N. J. Nanoshell-enabled photothermal cancer therapy: impending clinical impact. *Acc Chem Res* **41,** 1842-1851 (2008)

38. Jackson, J. D. *Classical electrodynamics* 3. edn(Wiley, New York, 1999)

39. Mie, G. Articles on the optical characteristics of turbid tubes, especially colloidal metal solutions. *Annalen Der Physik* **25,** 377-445 (1908)

40. Kittel, C. *Introduction to solid state physics* 8th edn(Wiley, Hoboken, NJ, 2005)

41. Johnson, P. B. & Christy, R. W. Optical constants of transition metals: Ti, V, Cr, Mn, Fe, Co, Ni, and Pd. *Physical Review B* **9,** 5056-5070 (1974)

42. Johnson, P. B. & Christy, R. W. Optical constants of the noble metals. *Physical Review B* **6,** 4370-4379 (1972)

43. Chen, X., Chen, Y., Yan, M. & Qiu, M. Nanosecond photothermal effects in plasmonic nanostructures. *ACS Nano* **6,** 2550-2557 (2012)

44. Marder, M. P. *Condensed matter physics* (Wiley, New York, 2000)

45. Kelly, K. L., Coronado, E., Zhao, L. L. & Schatz, G. C. The optical properties of metal nanoparticles: The influence of size, shape, and dielectric environment. *Journal of Physical Chemistry B* **107,** 668-677 (2003)

46. Bohren, C. F. & Huffman, D. R. *Absorption And Scattering Of Light By Small Particles* (Wiley, New York, 1983)

47. Meier, M. & Wokaun, A. Enhanced Fields on Large Metal Particles - Dynamic Depolarization. *Optics Letters* **8,** 581-583 (1983)

48. Wokaun, A., Gordon, J. P. & Liao, P. F. Radiation Damping in Surface-Enhanced Raman-Scattering. *Physical Review Letters* **48,** 957-960 (1982)

49. Heilweil, E. J. & Hochstrasser, R. M. Nonlinear spectroscopy and picosecond transient grating study of colloidal gold. *The Journal of Chemical Physics* **82,** 4762-4770 (1985)

50. Bosbach, J., Hendrich, C., Stietz, F., Vartanyan, T. & Trager, F. Ultrafast dephasing of surface plasmon excitation in silver nanoparticles: Influence

of particle size, shape, and chemical surrounding. *Physical Review Letters* **89,** (2002)

51. Link, S. & El-Sayed, M. A. Spectral Properties and Relaxation Dynamics of Surface Plasmon Electronic Oscillations in Gold and Silver Nanodots and Nanorods. *The Journal of Physical Chemistry B* **103,** 8410-8426 (1999)

52. Guillon, C., Langot, P., Del Fatti, N. & Vallée, F. Ultrafast surface plasmon resonance Landau damping and electron kinetics in metal nanoparticles. In: Tsen KT, Song JJ, Jiang H, editors.; 2004; San Jose, CA; 2004. p. 65-76.

53. Lee, J., Javed, T., Skeini, T., Govorov, A. O., Bryant, G. W. & Kotov, N. A. Bioconjugated Ag Nanoparticles and CdTe Nanowires: Metamaterials with Field-Enhanced Light Absorption. *Angewandte Chemie International Edition* **45,** 4819-4823 (2006)

54. Muskens, O. L., Giannini, V., Sánchez-Gil, J. A. & Gómez Rivas, J. Strong Enhancement of the Radiative Decay Rate of Emitters by Single Plasmonic Nanoantennas. *Nano Letters* **7,** 2871-2875 (2007)

55. Bauer, C., Abid, J.-P., Fermin, D. & Girault, H. H. Ultrafast chemical interface scattering as an additional decay channel for nascent nonthermal electrons in small metal nanoparticles. *The Journal of Chemical Physics* **120,** 9302-9315 (2004)

56. Christopher, P., Xin, H. & Linic, S. Visible-light-enhanced catalytic oxidation reactions on plasmonic silver nanostructures. *Nature Chemistry* **3,** 467-472 (2011)

57. Baffou, G. & Rigneault, H. Femtosecond-pulsed optical heating of gold nanoparticles. *Physical Review B - Condensed Matter and Materials Physics* **84,** (2011)

58. Govorov, A. O., Zhang, W., Skeini, T., Richardson, H., Lee, J. & Kotov, N. A. Gold nanoparticle ensembles as heaters and actuators: melting and collective plasmon resonances. *Nanoscale Research Letters* **1,** 84-90 (2006)

59. Baffou, G., Kreuzer, M. P., Kulzer, F. & Quidant, R. Temperature mapping near plasmonic nanostructures using fluorescence polarization anisotropy. *Optics Express* **17,** 3291-3298 (2009)

60. Baffou, G., Girard, C. & Quidant, R. Mapping heat origin in plasmonic structures. *Physical Review Letters* **104,** 136805 (2010)

61. Honda, M., Saito, Y., Smith, N. I., Fujita, K. & Kawata, S. Nanoscale heating of laser irradiated single gold nanoparticles in liquid. *Optics Express* **19,** 12375-12383 (2011)

62. Van de Broek, B., Grandjean, D., Trekker, J., Ye, J., Verstreken, K., Maes, G., Borghs, G., Nikitenko, S., Lagae, L., Bartic, C., Temst, K. & Van Bael, M. J. Temperature Determination of Resonantly Excited Plasmonic Branched Gold Nanoparticles by X-ray Absorption Spectroscopy. *Small* **7,** 2498-2506 (2011)

63. Stietz, F. Laser manipulation of the size and shape of supported nanoparticles. *Applied Physics a-Materials Science & Processing* **72,** 381-394 (2001)

64. Bird, R. E., Hulstrom, R. L. & Lewis, L. J. Terrestrial solar spectral data sets. *Solar Energy* **30,** 563-573 (1983)

65. Minkina, W. & Dudzik, S. *Infrared thermography : errors and uncertainties* (J. Wiley, Chichester, West Sussex, U.K. ; Hoboken, NJ, 2009)

66. Fredriksson, H., Alaverdyan, Y., Dmitriev, A., Langhammer, C., Sutherland, D. S., Zaech, M. & Kasemo, B. Hole-mask colloidal lithography. *Advanced Materials* **19,** 4297-4302 (2007)

67. Ohring, M. *Materials science of thin films : deposition and structure* 2nd edn(Academic Press, San Diego, CA, 2002)

68. Safi, I. Recent aspects concerning DC reactive magnetron sputtering of thin films: a review. *Surface and Coatings Technology* **127,** 203-218 (2000)

69. Flewitt, P. E. J. & Wild, R. K. *Physical methods for materials characterisation* 2nd edn(Institute of Physics Pub., Bristol ; Philadelphia, 2003)

70. Danilatos, G. D. Review and Outline of Environmental Sem at Present. *Journal of Microscopy-Oxford* **162,** 391-402 (1991)

71. Rodahl, M., Hook, F., Fredriksson, C., A. Keller, C., Krozer, A., Brzezinski, P., Voinova, M. & Kasemo, B. Simultaneous frequency and dissipation factor QCM measurements of biomolecular adsorption and cell adhesion. *Faraday Discussions* **107,** 229-246 (1997)

72. Höök, F., Vörös, J., Rodahl, M., Kurrat, R., Böni, P., Ramsden, J. J., Textor, M., Spencer, N. D., Tengvall, P., Gold, J. & Kasemo, B. A comparative study of protein adsorption on titanium oxide surfaces using in situ ellipsometry, optical waveguide lightmode spectroscopy, and quartz crystal microbalance/dissipation. *Colloids and Surfaces B: Biointerfaces* **24,** 155-170 (2002)

73. *ThermoVision™A20 V, Operator's manual* a72 edn. [cited 9 April 2013] Available from: www.flir.com

74. Johnson, D., Hilal, N. & Bowen, W. R. Chapter 1 - Basic Principles of Atomic Force Microscopy. *Atomic Force Microscopy in Process Engineering*. Butterworth-Heinemann: Oxford, 2009, pp 1-30.

75. Ghoshdastidar, P. S. *Heat transfer* 2nd edn(Oxford University Press, New Delhi, 2012)

76. Tong, L., Pakizeh, T., Feuz, L. & Dmitriev, A. Highly directional bottom-up 3D nanoantenna for visible light. *Sci. Rep.* **3,** (2013)